Theoretical and Applied Climatology (2024) 155:7095–7108
https://doi.org/10.1007/s00704-024-05056-9

RESEARCH

Dynamic and thermodynamic characteristics of warm-sector rainstorms caused by the southwest china vortex in sichuan basin

Chunhua Zhou[1,3] · **Yueqing Li**[1,2]

Received: 4 March 2024 / Accepted: 5 June 2024 / Published online: 12 June 2024

Abstract

Using automatic rainfall station and ERA5 reanalysis data, the Southwest China vortex (SWCV) processes that induce warm-sector rainstorms in the Sichuan Basin were analyzed, their environmental field and dynamic thermal characteristics were researched through physical diagnosis and dynamic synthesis, and the development mechanism was discussed. The results showed that for the warm-sector rainstorms caused by the SWCV (SWCV-WR), the general circulation backgrounds ~~can~~ could be divided into three types: upper trough-vortex (Type I), plateau shear line (Type II), and short-wave trough (Type III) types. Regarding the aspects of the maintenance of the SWCV, duration of the warm-sector rainstorms, and maximum hourly precipitation intensity, the influence of Type I is the most evident, followed by Types II and III for SWCV-WR. The vertical structure of the SWCV is shallow and inclined to the west with height, but the positive vorticity of Types I and II can reach up to 200 hPa for SWCV-WR. The pseudo-equivalent potential temperature in the vortex area is greater than 354 K, which is accompanied by an upward-energy tongue, and shallow secondary circulation occurs on the eastern side of the SWCV, promoting vortex development. Regarding the thermodynamic characteristics of SWCV, Type I is the strongest, followed by Type III, and Type II is the weakest. The water vapor supply in different types of SWCV-WR is not only closely related to the strength of water vapor transport in the Bay of Bengal, but also to the variations in water vapor transport caused by the influence of different water vapor sources, such as the South China Sea and western Pacific Ocean, during its transportation. For SWCV-WR, the vorticity advection presents an uneven east-west positive and negative distribution. Under the dynamic forcing, the positive vorticity on the east side of SWCV of Types I and II (III) is enhanced (weakened), while that on the west side is weakened (enhanced). Different atmospheric vorticity variations have different significant effects on the three types of SWCV-WR. Under the spatial non-uniform heating, the horizontal non-uniform heating effect on the different types of SWCV-WR has regional differences, while the vertical non-uniform heating effect has the largest effect on the spatial non-uniform heating and a positive heating effect on the three types of SWCV-WR. Therefore, the spatial non-adiabatic heating effect, particularly the vertical non-uniform heating effect, is an important mechanism for the development and evolution of SWCV and SWCV-WR.

1 Introduction

The Southwest China vortex (SWCV) is a low-pressure system with cyclonic circulation over 700 or 850 hPa, and it is generated in the southwestern region of China under the influence of the Qinghai-Tibet Plateau topography. It has a diameter of 300–500 km and a life history of 48 h. Some of the eastward developments can last for more than seven days. There are three main large-scale vortex sources: the Jiulong vortex source in the southern part of the western Sichuan Plateau, the Xiaojin vortex source in the central part of the western Sichuan Plateau, and the western Sichuan Basin vortex source in the eastern part of the Qinghai-Tibet Plateau. Most of the SWCV is cold, whereas some areas

✉ Yueqing Li
yueqingli@163.com

[1] Heavy Rain and Drought-Flood Disasters in Plateau and Basin Key Laboratory of Sichuan Province, Chengdu 610072, China

[2] Institute of Plateau Meteorology, CMA, Chengdu 610072, China

[3] Sichuan Meteorological Disaster Prevention Technology Center, Chengdu 610072, China

are warm or warm at origin and subsequently become cold (Li 2021). The SWCV is an important weather system that affects rainstorms in China. Once the SWCV moves out, it brings about severe rainstorms and flood disasters to the vast areas of China , and the intensity and scope of its impact are second only to those of typhoons and their residual low pressure. Moreover, most rainstorms in the Sichuan Basin are related to the SWCV (Zhou and Xiao et al. 2022). As SWCV is warm at its origin, precipitation under the influence of the SWCV often exhibits the characteristics of warm-sector rainstorms. According to statistics, SWCV warm-sector rainstorms account for 30% of warm-sector rainstorms in the Sichuan Basin (Xiao et al. 2020; Xiao et al. 2021), representing the main impacting system. The SWCV and its associated rainstorms have long been the focus and a complication of meteorological scientific research and operational forecasting.

Research on the SWCV has a history of nearly 80 years, and many significant achievements have been made in the formation of the source of SWCV, the formation, development, and extinction mechanisms, the evolution process after moving out of the vortex source, and the mechanism of the influences of weather, such as heavy precipitation (Chen et al. 2015; Chen and Li 2022; Hu et al. 2021; Li 2021; Li et al. 2022; Liu et al. 2022; Wang and Liu 2017; Yu et al. 2022; Zhou et al. 2017; Zhang et al. 2019; Zhao et al. 2023). In recent years, satellite data have been used to explore southwest eddy precipitation (Chen et al. 2021; Mao et al. 2023). However, studies of the SWCV and warm-sector rainstorms in Sichuan, mainly focused on typical cases and their feature characteristics, are scarce. For example, in a case study, Zong et al. (2013) compared and analyzed the Mesoscale Convective System(MCS) activity characteristics and environmental fields of the warm-sector rainstorms in the Sichuan Basin caused by the two southwest vortices, and determined and compared their MCS activity characteristics. Yang et al. (2017) analyzed the mesoscale characteristics and trigger mechanism of a warm-sector rainstorm in the Sichuan Basin under the influence of the Tibetan Plateau vortex (TPV) and revealed the reason underlying the long duration of the warm-sector rainstorm process. Huang et al. (2022) studied the dynamic and thermal structural characteristics and topographic effects of a warm-sector rainstorm at night and reported the water vapor, dynamic and thermal evolution, and triggering mechanism characteristics of a warm-sector rainstorm under the influence of weak weather-scale forcing and special topography. Based on observations and analysis, Luo et al. (2020) calculated the radar echo characteristics of different rainfall types before and after the maturation of warm-sector rainstorms in the Sichuan Basin. Meanwhile, Bian and Li (2024) conducted a statistical analysis of the characteristics of convective cloud clusters of the rainstorms in the southwest vortex-type warm sector of Liangshan Prefecture, Sichuan Province. Regarding environmental field characteristics, Xiao et al. (2020, 2021) analyzed the spatiotemporal distribution characteristics and related physical quantity thresholds of sudden warm-sector rainstorms in the Sichuan Basin and classified the influencing systems. Although these achievements have enhanced our basic understanding of the distribution characteristics of warm-sector rainstorms in Sichuan, relatively little is known about their impact systems and evolution mechanisms. Further research on warm-sector rainstorms weather in the Sichuan Basin under the influence of SWCV is needed.

Owing to the blocking effects of the Qinghai-Tibet Plateau, Qinling Mountains, Daba Mountains, and other large-scale terrains, high-latitude cold air cannot easily directly invade the Sichuan Basin, and warm moisture flow from the south can easily accumulate in the region. Therefore, the Sichuan Basin becomes a significant "moisture sink" (Qi et al. 2021), which increases the frequency of warm-sector rainstorms in the summer. The SWCV is an important system that affects the occurrence of rainstorms in the warm sector (Xiao et al. 2020, 2021). However, the evolution of the SWCV system and its relationship with the occurrence and development of warm-sector rainstorms in the Sichuan Basin remain unclear. Therefore, this study focuses on the SWCV, which has induced warm-sector rainstorms in the Sichuan Basin for over 10 years, its environmental field and dynamic thermal structure characteristics, along with its maintenance and development mechanisms, are analyzed. The study findings elucidate the warm-sector rainstorm process in the Sichuan Basin under the influence of the SWCV and provide technical support for the prediction of rainstorms and other disastrous weather events.

2 Data and methods

2.1 Data

The data used in this study included the following: (1) rainfall data from automatic stations in Sichuan from 2012 to 2023 compiled by the Sichuan Meteorological Information Center; (2) MICAPS sounding observation data from China Meteorological Administration during 2012–2023; (3) the geospatial data cloud (https://www.gscloud.cn/) 90 m digital elevation model; and (4) ERA5, the fifth-generation atmospheric reanalysis data from the European Centre for Medium Range Weather Forecasts (ECMWF) during 1981-2023 (https://cds.climate.copernicus.eu/), which have 37 layers in the vertical direction, a horizontal resolution of 0.25° × 0.25°, and a time interval of 1 h. The data and analysis times in this study were all in Beijing time.

2.2 Methods

The vorticity budget equation has been widely used in the diagnosis and analysis of low-pressure systems such as SWCV and TPV as well as their precipitation events. On this basis, the environmental field, dynamic characteristics, and development mechanism of the SWCV-induced warm-sector rainstorm in the Sichuan Basin are discussed. The vorticity budget equation in the P-coordinate system is as follows (Zhang 1992):

$$\frac{\partial \zeta}{\partial t} = -\left(u\frac{\partial \zeta}{\partial x} + v\frac{\partial \zeta}{\partial y}\right) - v\frac{\partial f}{\partial y} - \omega\frac{\partial \zeta}{\partial p} + \left(\frac{\partial \omega}{\partial y}\frac{\partial u}{\partial p} - \frac{\partial \omega}{\partial x}\frac{\partial v}{\partial p}\right) - (f+\zeta)\left(\frac{\partial u}{\partial x} + \frac{\partial v}{\partial y}\right) \quad (1)$$

The items on the right side of Formula (1) are the vorticity horizontal advection, vertical transport, horizontal divergence, and torsion terms.

Using a complete-form vertical vorticity tendency equation to explore the influence of diabatic heating on vorticity, the equation in the P-coordinate system is as follows (Liu et al. 1999; Wu et al. 1999):

$$\frac{\partial \zeta}{\partial t} = -V\cdot\nabla\zeta - \beta v + (1-k)\cdot(f+\zeta)\frac{\omega}{p} - (f+\zeta)\frac{Q}{\theta} + \frac{f+\zeta}{\theta_z}\frac{\partial Q}{\partial z} - \frac{1}{\theta_z}\frac{\partial v}{\partial x}\frac{\partial Q}{\partial x} + \frac{1}{\theta_z}\frac{\partial u}{\partial y}\frac{\partial Q}{\partial y} \quad (2)$$

The items on the right side of formula (2) are the vorticity advection, β effect term, ascending motion, heat source, vertical non-uniform heating, and horizontal non-uniform heating terms.

The calculation of the diabatic heating rate can be obtained by the "inverse calculation method" and its formula is as follows (Yanai et al. 1973):

$$Q = \frac{Q_1}{C_p} = \left(\frac{\partial T}{\partial t} + V\cdot\nabla T + \left(\frac{P}{P_0}\right)^k \omega\frac{\partial \theta}{\partial p}\right) \quad (3)$$

Where u and v are the zonal and meridional horizontal wind speed, ω is the vertical wind velocity in the pressure coordinate, ζ is the relative vorticity; f is the Coriolis parameter, θ is the potential temperature;$\theta_z = \frac{\partial \theta}{\partial z}$,$Q_1$ is the diabatic heating; Q is the diabatic heating rate, which is calculated by formula (3); C_p is the specific heat at constant pressure, and it has a value of 1004.8416 J/(kg.K); T is the temperature; and V is the horizontal vector wind field, k=0.2875, P_0=1000 hPa.

According to scale analysis(Wu et al. 1999), the magnitude of the vorticity advection term in Formula (2) is $10^{-10}s^{-2}$, the magnitude of the β effect term is $10^{-10}s^{-2}$, the magnitude of the heat source is $10^{-10}s^{-2}$, and the magnitude of the spatial non-uniform heating effect is 10^{-9} s^{-2}. Therefore, based on the spatially non-uniform heating effect, the environmental field, thermal characteristics, and development mechanism of the SWCV-induced warm-sector rainstorms in Sichuan Basin are discussed.

2.3 Dynamic synthesis method

To avoid the average attenuation of warm-sector rainstorm characteristics in the Sichuan Basin by case synthesis, dynamic synthesis was used for the analysis. The specific methods used are as follows (Gray 1981):

(4)

$$\overline{S}_t(x,y) = \frac{1}{N}\sum_{n-1}^{N} S_t(x,y)$$

Where $\overline{S}_t(x,y)$ is the sample mean-field, $S_t(x,y)$ is the physical field at time t, and N is the total number of samples. The geometric center of each SWCV wind field at 850 hPa was regarded as the central coordinate (0,0), and the grid points within 10° × 10° were used for the dynamic synthesis of the arithmetic average of the physical quantity field. The zonal relative coordinates from left to right represent west to east, represented by x/longitude on the graph, while the meridional relative coordinates from bottom to top represent south to north, represented by y/latitude.

2.4 Specific definitions and case selection

A warm-sector rainstorm in the Sichuan Basin is defined as follows (Xiao et al. 2020, 2021): Precipitation occurs in the warm sector at least 100 km away from the front of the surface cold front or in the thermal low-pressure circulation area and is not affected by the cold air on the ground when it occurs, and there is no cold advance flow into the rainfall area at 850 hPa. The Sichuan Basin has a rainfall process occurring in three or more adjacent national stations, or five or more scattered national stations with≧50 mm daily precipitation in each station, and is accompanied by short-term heavy precipitation (≧20 $mm.h^{-1}$).

The SWCV is defined as follows: as the SWCV-WR is shallow, referring to the existing standard (Li 2021). This study refers to the complete vortex with cyclonic wind direction on the leeward slope of the Qinghai-Tibet Plateau (99-109 ° E, 26-33 ° N) on the 850 hPa isobaric surface as the SWCV.

The warm-sector rainstorm processes caused by SWCV (referred to as SWCV-WR) are defined based on the above warm-sector rainstorm standard in the Sichuan Basin, the

direct impact system is SWCV in 850hPa for the warm-sector rainstorm process.

According to the above definition standards, the ERA5 850 hPa wind field data were used to select individual cases affected by the SWCV. Combined with the positive pressure and negative temperature of surface pressure, as well as the 850 hPa cold advection situation, the warm-sector period of the SWCV was defined. Then, the rainfall data of automatic stations were used to select cases that met the rainfall standards. According to statistics , 17 SWCV-WR cases have occurred in Sichuan from 2012 to 2023 (Table 1). The influence system of the lower troposphere (850 hPa) of the SWCV-WR is the SWCV, however, the middle troposphere (500 hPa) can be influenced by other weather circulation systems. Therefore, using 500 hPa main impact systems closest to the rainstorm center when the rainstorm occurs in the warm-sector as the basis for further classification. 17 SWCVWRs were divided into three types: upper-level trough-vortex type (Type I, with five cases), plateau shear line type (Type II, with five cases), and short-wave trough type (Type III, with seven cases). The characteristics of the three SWCV-WR types are as follows.

Type I: The main impact system is the upper-level trough and the eastward-moving TPV merging into the upper-level trough. The source region of the SWCV is in the Sichuan Basin. The average duration of the SWCV-WR is 20 h, and the average duration of the SWCV system is 76.8 h, resulting in an average maximum hourly rainfall intensity of 96.8 mm.

Type II: The main impact system is the plateau shear line. The source region of the SWCV is mostly in Jiulong County. The average duration of the SWCV-WR is 15.6 h, and the average duration of the SWCV system is 74.2 h, resulting in an average maximum hourly rainfall intensity of 81.14 mm.

Type III: The main impact system is the plateau short-wave trough. The source region of the SWCV is in the Sichuan Basin. The duration of the SWCV-WR is 17.1 h, and the average duration of the SWCV system is only 31.2 h, resulting in an average maximum hourly rainfall intensity of 84.2 mm.

3 SWCV-WR circulation background

For the SWCV-WR, the general circulation in the mid-upper troposphere is as follows: in the 500 hPa subtropical high of Type I distributed in a "block" shape in the western Pacific Ocean (Fig. 1a, d), with the 588 dagpm line west-extending point at 115° E and the ridge line near 28.5° N, thus forming a blocking effect is formed in eastern China, where the upper-level trough and TPV of influencing Sichuan move slowly eastwards. The Sichuan Basin is controlled by warm and humid airflow in front of the upper-level trough and TPV. The positive vorticity advection in front of the trough promotes the generation and development of the SWCV, and the temperature field on the Qinghai-Tibet Plateau is a warm zone of 272 K. The South Asian high is intense at 200 hPa, and the Sichuan

Table 1 SWCV-WR cases

Category	Time period of SWCV-WR occurrence (yyyymmddhh-ddhh)	Duration of SWCV/Duration of SWCV-WR (unit: h)	SWCV-WR maximum cumulative rainfall/maximum hourly rainfall intensity (unit: mm)	Strongest moment(yyyymmddhh) and geometric center position of SWCV at 850 hPa
Type I	2012070216-0317	77/26	181/68.9	2012070305 (104.5°E,29.5°N)
	2013062908-3005	97/22	244.3/95.5	2013063003 (104.5°E,29.8°N)
	2020081101-1117	67/17	373.6/156.8	2020081111 (104.5°E,29°N)
	2021070918-1008	86/14	161.5/59.9	2021071006 (105°E,30.8°N)
	2023072600-2620	57/21	230.3/102.9	2023072617 (104.75°E,29.75°N)
Type II	2014081622-1720	71/23	174.6/49	2014081708 (105.8°E,29.4°N)
	2018063000-3008	30/9	232.7/103.1	2018063003 (105.5°E,30.3°N)
	2018070206-0217	107/12	284.8/107.8	2018070206 (104.4°E,29.5°N)
	2020071000-1020	93/21	169.8/54.1	2020071014 (105°E,29.8°N)
	2021082117-2205	70/13	127.6/91.7	2021082204 (104.5°E,30.5°N)
Type III	2014060223-0315	17/17	252.7/103.8	2014060303 (105°E,28.3°N)
	2014080404-0411	8/8	172/63.3	2014080404 (104.5°E,28.5°N)
	2020061600-1613	37/14	290.4/107.2	2020061607 (104.7°E,31°N)
	2020071418-1520	63/27	279.8/79.7	2020071504 (104.5°E,29.5°N)
	2020072405-2418	28/14	189.3/63.2	2020072406 (105°E,31°N)
	2021081623-1716	18/18	178/86.9	2021081705 (104.4°E,30°N)
	2021091419-1517	48/22	188.1/85.2	2021091512 (104.5°E,30.5°N)

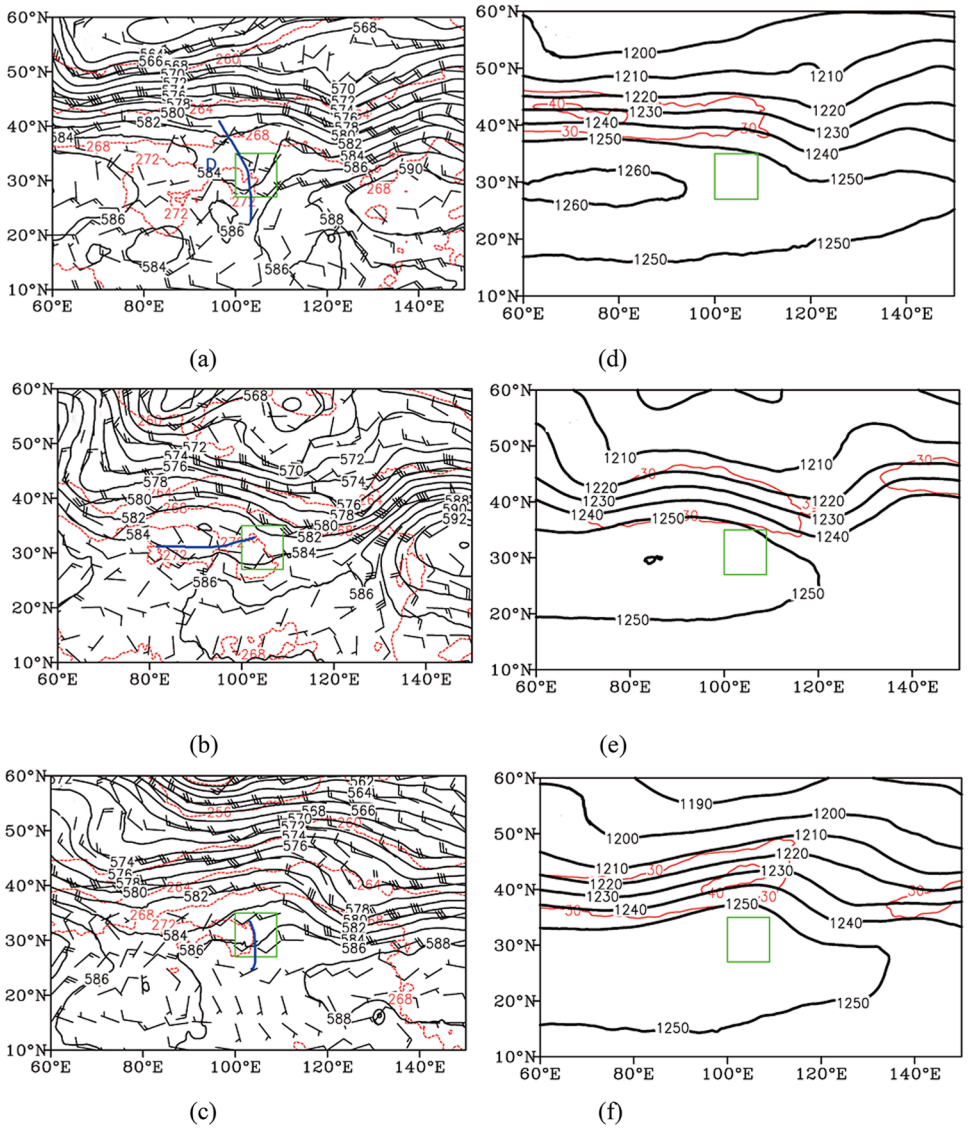

Fig. 1 Height field at 500 hPa (**a-c**, black contour, unit: dagpm), temperature field (**a–c**, red dotted line, unit: K) and wind field (barb), height field at 200 hPa (d–f, black contour, unit: dagpm), and zonal wind (**d–f**, red contour is≧30m/s, unit: m/s): (**a, d**) Type I; (**b, e**) Type II; (**c, f**) Type III. The blue solid line is the trough line (shear line) of the 500 hPa main influence system, the blue "D" represents the TPV position, and the green box represents the key research area

Basin is on the left side of the upper-level jet outlet and in the divergence zone behind the upper-level cold trough, which is conducive to the SWCV's development. The subtropical high of Type II is stronger than those of Types I and III, and is located more easterly and northerly (Fig. 1b, e), with the 588 dagpm line west-extending point at 131°E and the ridge line near 32°N. The Sichuan Basin is affected by the eastern section of the plateau shear line, and the temperature field from the Qinghai-Tibet Plateau to the Sichuan Basin is a warm zone of 272 K. The general circulation at 200 hPa is similar to that of Type I, although the intensity of the South Asian high is slightly weak. The subtropical high of Type III is more southerly than those of Types I and II(Fig. 1c, f) and has an east-west zonal distribution. The ridge line is located near 22°N and has no blocking effect on the mid-latitude weather systems. This causes multiple short-wave troughs on the Qinghai-Tibet Plateau to move eastward, and the Sichuan Basin is affected by the southwest warm-humid airflow in the front of short-wave troughs. The circulation at 200hPa is similar to the first two types, but the intensity of the upper-level jet is relatively strong.

4 Rainfall intensity and environmental field characteristics of SWCV-WR

Figure 2 shows the spatial distribution of stations with SWCV-WR of 1 h≧50 mm. From this, Type II stations with 1 h≧50 mm are the most common, with an average of 43.4 stations per process. Heavy rainfall is mainly distributed in the southwest of the Sichuan Basin. Type III stations with 1 h≧50 mm are the second most common, with an average of 24.4 stations per process, heavy rainfall is mainly distributed in the northwest, center, and the

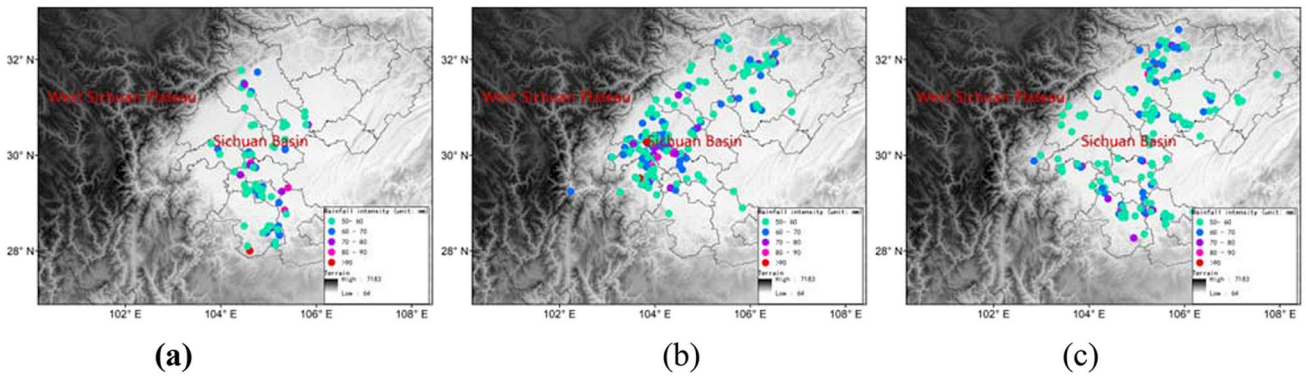

Fig. 2 Distribution of the SWCV-WR rainfall intensity. (**a**) Type I; (**b**) Type II; (**c**) Type III

southeast of the area. The fewest stations are of Type I with 1 h≧50 mm, and an average of 18.2 stations per process, heavy rainfall is mainly distributed in the southeast of the Sichuan Basin.

According to the sounding data statistics from the neighboring stations at 20 h before SWCV-WR, the three types of SWCV-WR all show regional high-energy instability. The average values of the various physical parameters of the environmental field (Table 2) reveal that before the warm-sector rainstorm, a large amount of convective available potential energy (CAPE) and a small amount of convective inhibition (CIN) occurs. The CIN value is much lower than that of CAPE, indicating that there is potential instability before SWCV-WR. The K index, A index, and uplift index (LI) induces also reflect the warm-humid atmosphere in the lower layer. The air mass is in an unstable stratification state, and the strong weather threat index(SWEAT) is above 238, which further indicates the strong convection characteristics of the SWCV-WR. Meanwhile, the level of free convection (LFC) and lift condensation level (LCL) are relatively low, and the easy-triggering characteristics of strong convection are also observed. Compared with the non-warm-sector rainstorms, the water vapor and energy conditions of SWCV-WR are significantly higher (Xiao et al. 2020; Xiao et al. 2021).

The southwest maximum wind speed zone with a wind speed of ≧ 12 m/s at 850 hPa or 700 hPa is called a low-level jet (LLJ). The characteristics of the LLJ in 17 SWCV-WR cases were investigated. The results reveal that 68.6% is accompanied by LLJ at 850hPa, and only 22.9% is accompanied by LLJ at 700hPa. This shows that the LLJ in the lower troposphere is important for SWCV-WR.

5 Water vapor transport characteristics of SWCV-WR

The Lagrangian Hybrid Single-Particle Orbit Model (HYSPLIT4) was used to analyze the water vapor transport of three types of SWCV-WR at 850 hPa (Fig. 3a), after 7 d of tracking, there are two water vapor transport paths for Types I and III, namely the Bay of Bengal and the South China Sea. Among them, Type I transports 67% of the trajectory from the Bay of Bengal to the Sichuan Basin, with water vapor transport contributing 64%, and 33% of the trajectory from the South China Sea to the northwest to reach the basin, with water vapor transport contributing 36%. A proportion of 64% of the Type III trajectories are transported northward from the northern South China Sea to the basin, with water vapor transport contributing 60%. Meanwhile, 36% of the trajectories are transported from the Bay of Bengal to the Sichuan Basin, with water vapor transport contributing 40%. All Type II trajectories are transported from the Bay of Bengal to the basin. Further analysis of the 850chPa water vapor flux divergence and water vapor flux anomaly reveals that the water vapor flux in the Sichuan Basin is $3\text{-}12\times10^{-2}$g. s^{-1}. cm^{-1}. hPa^{-1} higher than usual (Fig. 3b-d). At the same time, during the convergence and rise of water vapor in

Table 2 Average environmental parameter characteristics of SWCV-WR

Category	CAPE (J.kg^{-1})	K (°C)	LI (°C)	SWEAT	A	CIN (J.kg^{-1})	LCL (hPa)	LFC (hPa)	850 hPa LLJ frequency	700 hPa LLJ frequency
Type I	1990.36	38.06	-3.44	261.48	10.28	14.94	899.88	899.18	80%	20%
Type II	2386.03	39.86	-3.66	255.67	14.9	21.43	856.93	807.93	40%	20%
Type III	1426.74	40.66	-3.31	238.74	13.16	45.04	899.38	842.68	85.7%	28.6%

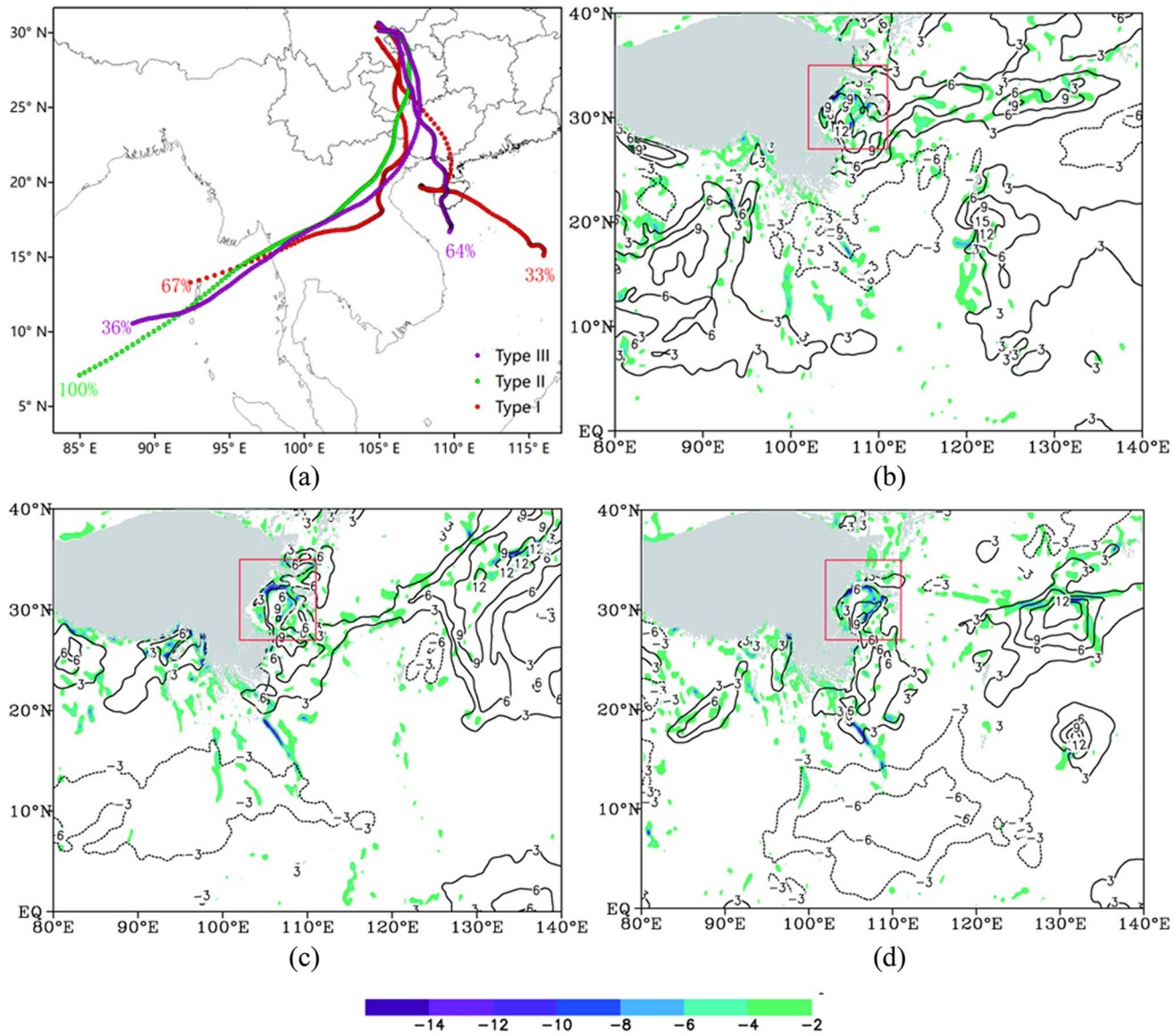

Fig. 3 The 850hPa water vapor trajectory and corresponding percentage (**a**), water vapor flux anomaly(contour, unit: 10^{-2} g.s^{-1}.cm^{-1}.hPa^{-1}) , and water vapor flux divergence(shading, displaying only negative values, unit:10^{-7}g.s^{-1}.cm^{-2}.hPa^{-1}) (**b-d**). (**b**) Type I; (**c**) Type II; (**d**) Type III. The red box represents the key research area, and the gray shadow represents the terrain of Qinghai-Tibet Plateau at 850hPa

the Sichuan Basin, Type I water vapor flux in the Bay of Bengal is 6-12×10^{-2}g. s^{-1}. cm^{-1}. hPa^{-1} higher than usual, while the water vapor flux in the South China Sea is 3-6×10^{-2}g. s^{-1}. cm^{-1}. hPa^{-1} lower than usual. Although the water vapor flux in the Bay of Bengal is 3-6×10^{-2}g. s^{-1}. cm^{-1}. hPa^{-1} less than usual, its specific humidity is still ranges between 12-13 g. kg^{-1} (Figure omitted). Regarding the two main sources of water vapor in type III, the water vapor flux in the northern South China Sea is stronger than usual by 3-6×10^{-2}g. s^{-1}. cm^{-1}. hPa^{-1}, while the water vapor flux in the Bay of Bengal is slightly lower than usual.

6 Dynamic and thermal characteristics of SWCV-WR

A pseudo-equivalent potential temperature above 348 K is an important condition for warm-sector rainstorms(Zhao et al. 2008). From this, the dynamic and thermal characteristics of SWCV-WR are analyzed based on the variations in the pseudo-equivalent potential temperature and vorticity. Figures 4 and 5 indicate that the wind fields on the east and west sides of the low vortex developed asymmetrically, with the intensity of the southern wind exceeding

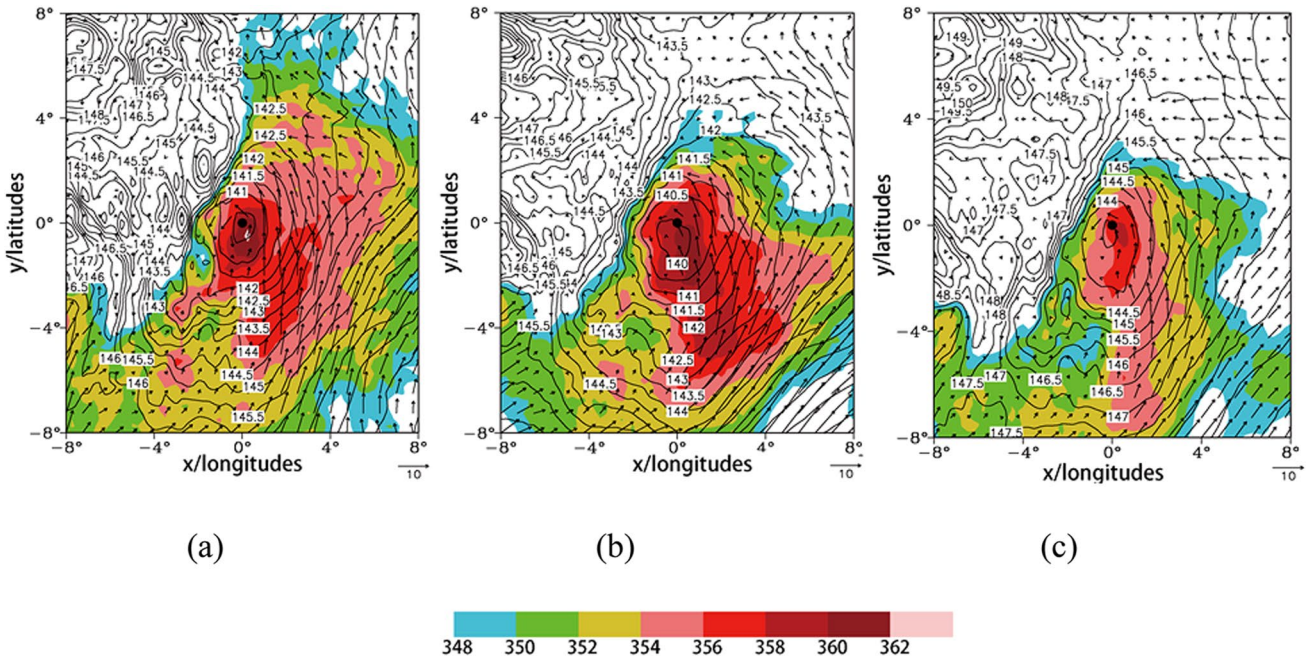

Fig. 4 Distribution of height field (contour, unit: dagpm), wind field (vector, unit: m/s), and pseudo-equivalent potential temperature (shading, unit: K) at 850hPa for SWCV-WR (the black dot is the synthetic SWCV center at 850hPa). (**a**) Type I; (**b**) Type II; (**c**) Type III

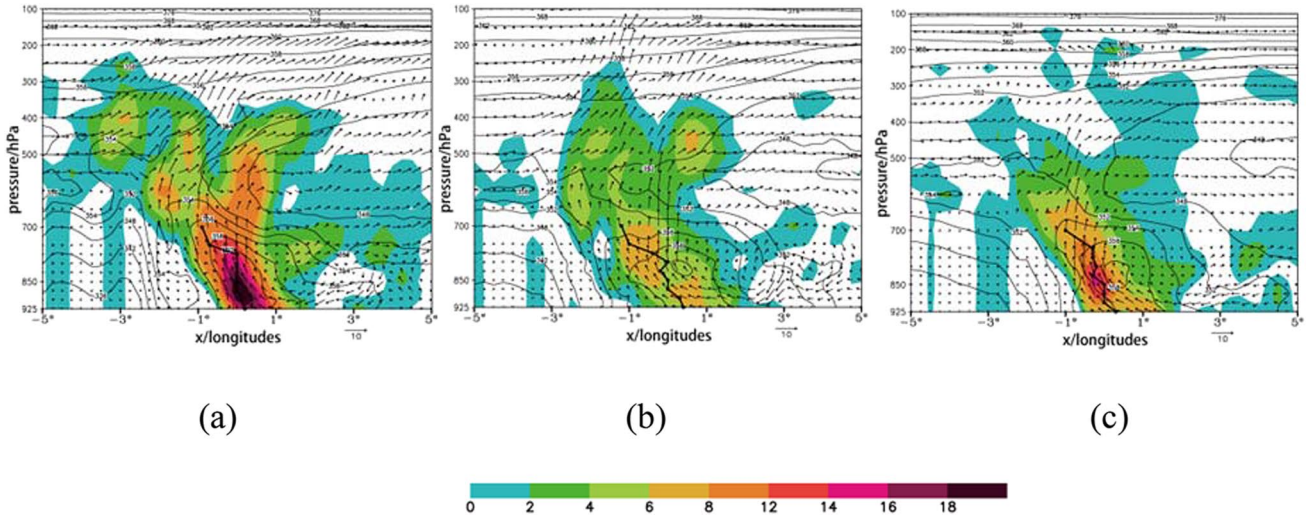

Fig. 5 Longitude-height profile distribution of pseudo-equivalent potential temperature (contour, unit: K), positive vorticity (shading, unit: 10^{-5}. s^{-1}), and u-w wind field synthesis (wind vector, unit: m/s) for SWCV-WR (black solid line represents the center profile of SWCV at different isobaric surfaces). (**a**) Type I; (**b**) Type II; (**c**) Type III

that of the northern wind. The pseudo-equivalent potential temperatures are all above 352 K, and the vortex center is the extreme region of the pseudo-equivalent potential temperature. In addition, shallow secondary circulation developed in the eastern part of SWCV. Among them, the southerly wind in the eastern part of SWCV is the strongest (Fig. 4a) in Type I, with a vortex intensity of 140.5 dagpm at 850 hPa and northeast-southwest elliptical distribution. As LLJ transports warm humid southwest air toward the low vortex, the pseudo-equivalent potential temperature extreme at the center of SWCV reaches 362 K. Additionally, SWCV tilts westwards with increasing geopotential height (Fig. 5a), accompanied by the development of an energy tongue, and convective instability occurs within SWCV. The distribution of vorticity profiles also showed the strongest positive vorticity intensity, with a center of

20×10^{-5} s^{-1}. Under the effect of positive vorticity advection in the front of the upper-level trough, the positive vorticity of SWCV vertically develops up to 200 hPa in the upper troposphere, becoming a deep low-vortex system. After the internal updraft reaches 600 hPa, it descends within approximately three longitudinal ranges in the eastern part of SWCV and then flows into SWCV, forming a shallow secondary circulation in the eastern part and promoting the development of SWCV. The southerly wind intensity in the eastern part of SWCV is the second-strongest (Fig. 4b and Fig 5b) in Type II. Although the intensity of the low vortex circulation center in 850 hPa reaches 140 dagpm, the intensity of the positive vorticity is the weakest, with an extreme intensity of only 8×10^{-5} s^{-1}. Moreover, owing to the forcing effect of upper-level shear lines, the positive vorticity of SWCV tilts and develops vertically, extending to the upper troposphere at 200 hPa. The pseudo-equivalent potential temperature extreme at the center of the low vortex is 360 K, and the range above 356 K is the widest with the development of an energy tongue. Similarly, there is a shallow secondary circulation in the eastern part of SWCV that promotes its development; however, the wind speed is weak. The SWCV circulation intensity at 850 hPa in Type III is the weakest (Fig. 4c, Fig. 5c), with a central intensity of only 143.5 dagpm, accompanied by the weakest southerly wind and pseudo-equivalent potential temperature. However, the positive vorticity intensity at the center of SWCV is close to that of Type I, with an extreme value of 16×10^{-5} s^{-1}. Owing to the weak forcing of the upper-level short-wave trough, the positive vorticity of SWCV is not sufficiently deep and only develops to approximately 400 hPa. The wind speed intensity of the shallow secondary circulation in the eastern part of SWCV is intermediate.

In addition, under the three different circulation backgrounds, the positive vorticity intensity that induced SWCV-WR was equivalent to the intensity that induced extreme rainstorms of SWCV in the Sichuan Basin (Zhou et al. 2022). However, the positive vorticity column of SWCV that induced extreme rainstorms mainly under dynamic action developed vertically, whereas the positive vorticity column of SWCV that induced warm-sector rainstorms developed slantingly westwards, with different vertical distributions.

7 Dynamic and thermal effect of SWCV-WR

7.1 Dynamic effect of SWCV-WR

The specific effect of atmospheric dynamic forcing on SWCV-induced warm-sector rainstorm events is discussed using the vorticity equation. As shown in Fig. 6, the distribution of the items affecting local vorticity changes is not uniform in the low-vortex region, and the distribution is positive-negative asymmetric in the east-west direction bounded by the center of the SWCV. The horizontal advection term (Fig. 6a–c) is negative on the east side and positive on the west side of SWCV, resulting in a reduction in the positive vorticity on the east side and an increase in the positive vorticity on the west side. The intensity of the horizontal advection term is strongest in Type I, followed by Type III; however, that of Type II is not significant. The distribution of the vertical transport term is similar to that of the torsion term (contours in Fig. 6a-c, shading in Fig. 6d–f), both of which are due to the uneven distribution of vorticity caused by the vertical motion, resulting in local vorticity variations. The two terms also exhibited positive-negative asymmetric distribution in the quasi east-west direction, but their effects are opposite to those of the vorticity advection term, which are positive on the east side of SWCV and negative on the west side. The positive vorticity transport intensity on the east side is strongest for Type I, followed by Type II and Type III is the weakest. For negative vorticity transport on the west side, the vertical transport term of Type III is the strongest, followed by Type I, and Type II is the weakest. The torsion term is strongest in Type I, followed by Type II; that in Type III is the weakest. However, the distribution of the horizontal divergence term is slightly different (contours in Fig. 6d–f). Type I is similar to the horizontal advection term, exhibiting positive-negative distribution in quasi east-west direction, with a negative value on the east side of SWCV and a positive value on the west side. In Type II, the SWCV region is positive, resulting in an increase in local vorticity within the low vortex. In Type III, the center and west side of SWCV have positive values, while the east side has weak negative values.

In summary, the effects of the different vorticity variations on SWCV in the low-vortex region of SWCV-WR are not uniform. The vertical transport and torsion terms of the vorticity equation strengthen the local vorticity on the east side of SWCV and attenuate it on the west side, whereas the vorticity advection term has the opposite effect. The combined effects of these factors are shown in Fig. 6g–i. Type I causes an increase in the local vorticity in the SWCV region, Type II causes an increase in the local vorticity in the center and east side of SWV, and Type III causes an increase in the local vorticity on the west side of SWCV.

7.2 Thermal effect of SWCV-WR

Studies have shown that spatially non-uniform heating is conducive to a positive vorticity increase of SWCV (Liu et al. 1999). For SWCV-WR, the spatial non-uniform heating effect of Type I reaches 20×10^{-9} s^{-2} at 850hPa(Fig. 7a),

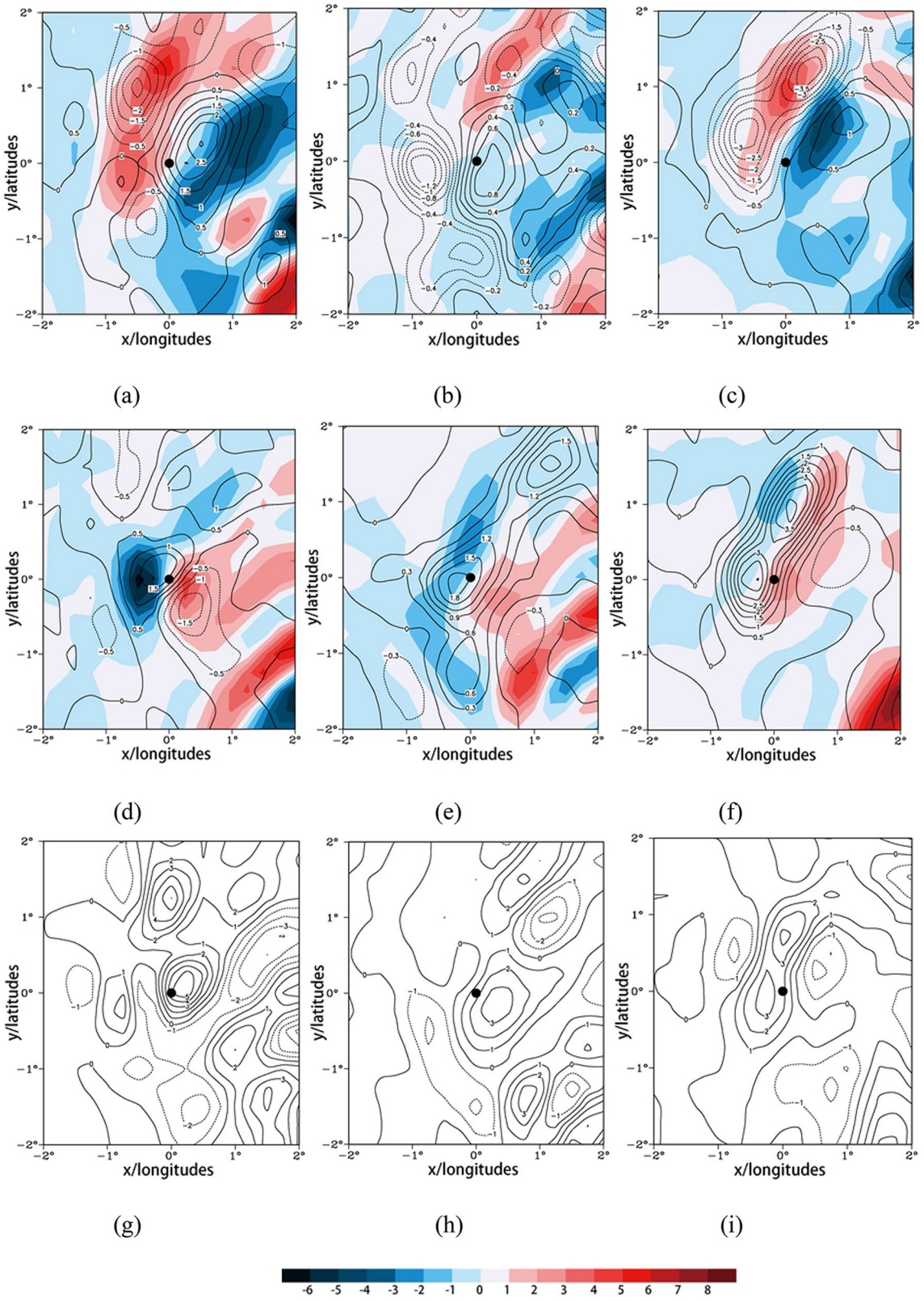

Fig. 6 Distribution of the vorticity advection term (**a–c**, shading), vorticity vertical transport term (**a–c**, contour), vorticity torsion term (**d–f**, shading), horizontal divergence term (**d–f**, contour), and vorticity local variation term (**g–i**, contour) at 850hPa for SWCV-WR (unit: 10^{-9} s^{-2}, black dots represent the center of SWCV at 850 hPa). (**a, d, g**) Type I, (**b, e, h**) Type II, (**c, f, i**) Type III

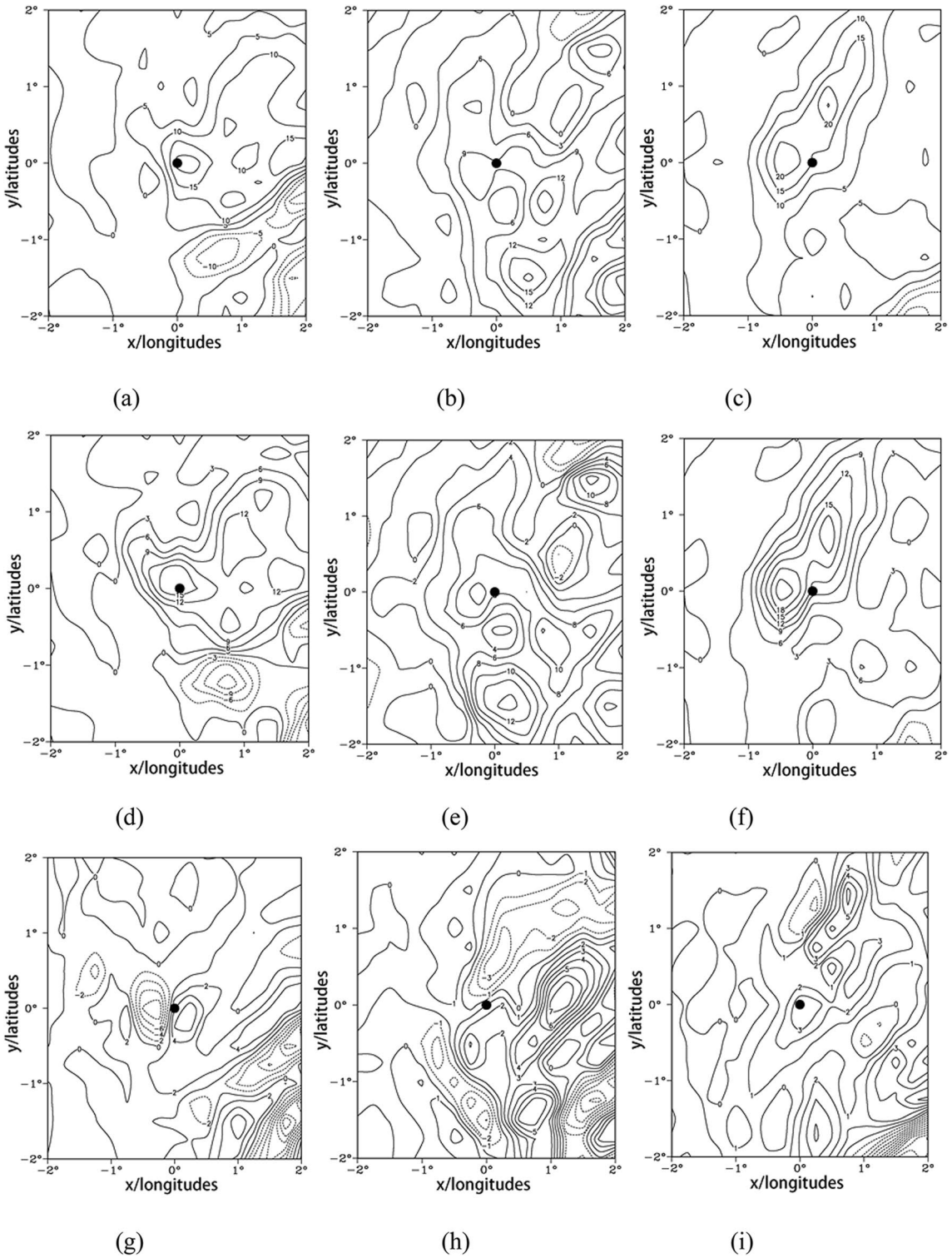

Fig. 7 Distribution of non-uniform heating terms (**a–c**), vertical non-uniform heating terms (**d–f**), and horizontal non-uniform heating terms (**g–i**) at 850 hPa for SWCV-WR (unit:10^{-9} s^{-2},black dots represent the center of SWCV at 850 hPa). (**a, d, g**) Type I, (**b, e, h**) Type II, (**c, f, i**) Type III.

the heating effect is mainly located on the east side of the SWCV, and the vertical non-uniform heating effect (Fig. 7d) is also observed in the SWCV region, with an extreme value of 15×10^{-9} s^{-2}, The horizontal non-uniform heating effect is heating on the east side of the SWCV reaching 6×10^{-9} s^{-2}, while it is the cooling effect on the west side reaching -8 $\times 10^{-9}$ s^{-2} (Fig. 7g), which strengthen the positive vorticity on the east side of the SWCV and weakens it on the west side. The final spatially non-uniform heating effect mainly occurs at the center and eastern side of the SWCV, which is conducive to its eastward movement and development. The spatial non-uniform heating effect of Type II is the weakest, with a value of only 9×10^{-9} s^{-2} (Fig. 7b). The vertical non-uniform heating effect all exists entirely in the SWCV region (Fig. 7e), while the horizontal non-uniform heating effect exert a negative cooling effect in the northern part of the SWCV and positive heating effect in the southern part (Fig. 7h). Ultimately, the high-value area of the spatially non-uniform heating effect is on the southern side of the SWCV, which is conducive to its southward movement and development. The spatial non-uniform heating effect of Type III is the strongest (Fig. 7c), with the extreme center located on the west and north sides of the SWCV reaching 20×10^{-9} s^{-2} and the extreme value of the vertical non-uniform heating effect reaching 21×10^{-9} s^{-2}(Fig. 7f). The horizontal non-uniform heating effect is all positive in the SWCV region (Fig. 7i), which ultimately lead to the extreme value of the spatial non-uniform heating effect mainly located in the northern part of the SWCV center, which is conducive to its northward movement and development.

8 Conclusion and discussion

Using 12-year reanalysis and rainfall data from 2012 to 2023, the SWCV-WR process was defined in the Sichuan Basin, individual cases of SWCV-WR were classified and analyzed statistically, and the environmental field and the dynamic thermal characteristics of the SWCV-WR were studied. The vorticity equation is used to research the occurrence and development of the physical mechanisms of the SWCV-WR. The following conclusions were drawn.

(1) The SWCV-WR process in the Sichuan Basin occurs in a high-energy and high-humidity atmospheric environment under three types of general circulation. The average duration of the SWCV under the influences of Types I and II is over 3 d, at 76.8 and 74.2h, respectively, whereas that of Type III only lasts for 1.5 days at 31.2h. The average durations of the SWCV-WR for Types I, III, and II are 20, 17.1 and 15.6 h, respectively. The maximum hourly rainfall intensity of SWCV-WR is the strongest in Type I, at 96.8 mm, followed by Types III and II , at 84.2 and 81.14 mm, respectively. Under the background of the different classified circulations, there are differences in the maintenance, duration, and precipitation intensity of the SWCV and SWCV-WR differ.

(2) The SWCV that causes warm-sector rainstorms is generally a shallow system located in the lower troposphere and inclines westwards with the height, however, the positive vorticity can extend to the upper troposphere, particularly under Types I and II. The pseudo-equivalent potential temperature in the SWCV region is above 354 K, and the energy tongue occurs correspondingly as the height increases. A shallow secondary circulation exists on the east side of the SWCV, which promotes its development. The central potential height intensity of the SWCV is strongest ~~in~~ under Type II, followed by Type I, and it is weakest under Type III. However, in terms of the dynamical and thermal characteristics, Type I is the strongest, followed by Type III, and Type II is the weakest, with the significant differences between the three types being significant.

(3) The water vapor transport of the SWCV-WR is closely related to the source areas of the Bay of Bengal, and the South China Sea. Type I water vapor mainly originates from the Bay of Bengal, followed by the South China Sea. Type II water vapor source is the Bay of Bengal. Type III water vapor mainly originates from the South China Sea, followed by the Bay of Bengal.

(4) For the warm-sector rainstorm, the vorticity advection transport in each quadrant of the SWCV circulation is not uniform, and it is mainly followed a positive-negative distribution in quasi east-west direction. The horizontal advection and torsion terms of vorticity strengthen the positive vorticity on the west side of the SWCV and attenuate it on the east side, while the vertical transport and horizontal divergence terms are opposite, causing positive vorticity to decrease on the west side of the SWCV and to increase on the east side, respectively. The dynamic forcing effect strengthens the positive vorticity on the east side of SWCV and weakens it on the west side for Types I and II, whereas the opposite is true for Type III, which strengthens the positive vorticity on the west side of the SWCV and weakens it on the east side. Different vorticity variation processes have different effects on the SWCV and SWCV-WR, and the dynamic effects on SWCV-WR exhibit regional differences under different types of general circulation.

(5) Diabatic heating has a significant impact on the SWCV-WR and is an important mechanism for its development and evolution. The spatially non-uniform heating strengthens the positive vorticity on the east side of SWCV for Type I and on the west side of the SWCV for Type III, respectively, while the spatially non-uniform heating effect distribution of the SWCV for Type II is relatively uniform. Vertical non-uniform heating has the greatest effect on spatial non-uniform heating, and all three types of SWCV-WR have positive heating effects. However, the distribution of the horizontal non-uniform heating effects is inconsistent,

and there is a clear regional difference for different types of heating effects.

In this study the SWCV-WR processes in the Sichuan Basin, the environmental field, and dynamic and thermodynamic characteristics over the past 12 years were analyzed. The development mechanism of the SWCV and its warm-sector rainstorm was preliminarily obtained. However, further in-depth research on the structural characteristics, anomalous evolution, and physical mechanisms of the SWCV-WR processes in the Sichuan Basin should be performed under the various circulation backgrounds based on a comprehensive diagnosis, numerical simulation, and other methods in the future.

Authorship contribution statement Chunhua Zhou: Conceptualization, Methodology, Software, Data collection and analysis, Writing-original draft preparation, Writing-reviewing and editing. Yueqing Li: Conceptualization, Project administration, Funding acquisition, Writing-reviewing and editing.

Formatting of funding sources This research was supported by the key project of Joint Meteorological Fund of the National Natural Science Foundation of China (grant no. U2242202), the key project of the National Natural Science Foundation of China (Grant No.42030611), and the Second Comprehensive Scientific Expedition to the Qinghai-Tibet Plateau is a national project(Grant No. 2019QZKK0103; 2019QZKK0105), the Innovative Development Special Project of China Meteorological Administration (CXFZ2023J016), the Innovation Team Fund of Sichuan Meteorological Administration (SCQXCXTD-202201).

Data availability No datasets were generated or analysed during the current study.

Declarations

Competing interest The authors declare no competing interests.

References

Bian Q, Li CH (2024) Statistical characteristics of torrential rain in the low vortex warm region of Southwest Liangshan experience in Sichuan . Journal of China west normal university(nature science). https://link.cnki.net/urlid/51.1699.n.20240105.1709.002

Chen KY, Fan J, Xian ZP (2021) Assimilation of MWHS-2/FY-3C 183 GHz channels using a dynamic emissivity retrieval and its impacts on precipitation forecasts: a southwest vortex case. Adv Meteorol 2021:1–14. https://doi.org/10.1155/2021/6427620

Chen YR, Li YQ (2022) A thermodynamic condition affecting the movement of a southwest China vortex case. Meteorol Atmos Phys 134:36. https://doi.org/10.1007/S00703-022-00874-W

Chen YR, Li YQ, Zhao TL (2015) Cause analysis on eastward movement of southwest China vortex and its induced heavy rainfall in south China. Adv Meteorol 2015:1–22. https://doi.org/10.1155/2015/481735

Gray WM (1981) Recent advances in tropical cyclone research from rawinsonde composite analysis. WMO Programme on research in Tropical Meteorology, Fort Collins, p 407

Hu Y, Liu HW, Liu HQ, Tang MH, Zeng YT (2021) Comparative analysis of two hazard rainstorm processes in Hunan affected by the Southwest China vortex. IOP Conf Ser :Earth Environ Sci 865:012032. https://doi.org/10.1088/1755-1315/865/1/012032

Huang CH, Li GP, Niu JL, Chen B, Chen G, Guo SY, Long KJ (2022) Dynamic and thermal structure and topographic impact of the night torrential rainfall in Lushan, Sichuan on August 10, 2020. Chin J Atmos Sci 46(4):989–1001. https://doi.org/10.3878/j.issn.1006-9895.2205.21205

Li C, Li Y, Fu SM, Jiang XW, Wang XF, Li SS, Cui CG, Hu Y, Cui WJ (2022) A new perspective on the orographic effect of the windward slope on the multi-scale eastward-Moving southwest vortex systems. Atmos Res 279:106365. https://doi.org/10.1016/j.atmosres.2022.106365

Li YQ (2021) New related progress on researches of the vortex source of Southwest China vortex. Plateau Meteor 40(6):1394–1406. https://doi.org/10.7522/j.issn.1000-0534.2021.zk005

Liu C, Li YQ, Liu ZM, Ye ML (2022) Physical formation mechanisms of the Southwest China vortex. Atmosphere 13(10):1546. https://doi.org/10.3390/atmos13101546

Liu YM, Wu GX, Liu H, Liu P (1999) The effect of spatially nonuniform heating the formation and variation of subtropical high Part III: Condensation heating and South Asia High and Western Pacific Subtropical High. Acta Meteor Sin 57(5):525–538. https://doi.org/10.11676/qxxb1999.051

Luo H, Xiao DX, Kuang QM, Qing Q, Kang L (2020) Radar echo characteristics and recognition of warm section torrential rain in Sichuan Basin. J Appl. Meteor Sci 34(4):460–470. https://doi.org/10.11898/1001-7313.20200408

Mao CY, Qing YY, Qian ZT, Zhang C, Gu ZH, Gong LQ, Liao JY, Li HW (2023) Application of FY satellite data in precipitation of eastward-moving Southwest China Vortex: A case study of precipitation in Zhejiang Province. Atmosphere 14(11):1664. https://doi.org/10.3390/atmos14111664

Qi DM, Li YQ, Zhou CY (2021) Variation characteristics of summer water vapor budget and its relationship with the precipitation over the Sichuan Basin. Water 13(18):2533. https://doi.org/10.3390/w13182533

Wang XM, Liu Y (2017) Causes of extreme rainfall in May 2013 over Henan Province: the role of the southwest vortex and low-level jet. Theor Appl Climatol 129:701–709. https://doi.org/10.1007/s00704-017-2054-4

Wu GX, Liu YM, Liu P (1999) The effect of spatially nonuniform heating on the formation and variation of subtropical highI: scale analysis. Acta Meteor Sin 57(3):257–263. https://doi.org/10.11676/qxxb1999.025

Xiao DX, Wang JJ, Cao PP, Lou H (2020) Characteristics and environmental conditions of the sudden warm-sector rainstorms in Sichuan Basin. J Nat Disasters 29(3):110–118. https://doi.org/10.13577/j.jnd.2020.0312

Xiao HR, Wang JJ, Xiao DX, Long KJ, Shen Y (2021) Analysis of warm-sector rainstorm characteristics over Sichuan Basin. Meteor Mon 47(3):303–316. https://doi.org/10.7519/j.issn.1000-0526.2021.03.004

Yanai M, Esbensen S, Chu JH (1973) Determination of bulk properties of tropical cloud clusters from large-scale heat and moisture budgets. J Atmos Sci 30:611–627. https://doi.org/10.1175/1520-0469(1973)030<0611:DOBPOT>2.0.CO;2

Yang KQ, Lu P, Zhang L (2017) Analysis of heavy rainstorm in warm sector under the influence of the low-pressure system of Qinghai-Xizang Plateau. J Trop Meteor 33(3):415–425. https://doi.org/10.16032/j.issn.1004-4965.2017.03.012

Yu SW, Zhang LF, Wang Y, Peng J (2022) Mesoscale horizontal kinetic energy spectra of an eastward-moving Southwest Vortex. Atmosphere 13(5):653. https://doi.org/10.3390/atmos13050653

Zhang DL (1992) The formation of a cooling-induced mesovortex in the trailing stratiform region of a midlatitude squall line. Mon Weather Rev 120:2763–2785. https://doi.org/10.1175/1520-0493(1992)120<2763:TFOACI>2.0.CO;2

Zhang YC, Fu SM, Sun JH, Fu R, Jin SL, Ji DS (2019) A 14-year statistics-based semi-idealized modeling study on the formation of a type of heavy rain-producing southwest vortex. Atmos Sci Lett 20:e894. https://doi.org/10.1002/asl.894

Zhao WL, Li YQ, Liu C, Peng JK (2023) Physical mechanism of the development and extinction of the China Southwest Vortex. Atmosphere 14(2):337. https://doi.org/10.3390/atmos14020337

Zhao YC, Li ZC, Xiao ZN (2008) Comparison analysis of South China front and warm-area heavy rain, systems in June 2006 cases. Meteor Sci Technol 36(1):47–54. https://doi.org/10.3969/j.issn.1671-6345.2008.01.009

Zhou CH, Xiao DX, Yu SH (2022) The circulation background and structural characteristics of the extreme rainstorm induced by the Southwest Vortex in Sichuan. Meteor Mon 48(12):1577–1589. https://doi.org/10.7519/j.issn.1000-0526.2022.081101

Zhou K, Liu HW, Zhao L, Zhu YX, Lin YH, Zhang FY, Fu N (2017) Binary mesovortex structure associated with southwest vortex. Atmos Sci Lett 18(6):246–252. https://doi.org/10.1002/asl.749

Zong ZP, Chen T, Xu J, Guan Y (2013) Analysis and forecast verification of two Southwest vortex torrential rain event in Sichuan Basin in early Autumn of 2012. Meteor Mon 39(5):567–576. https://doi.org/10.7519/j.issn.1000-0526.2013.05.004